



The role of phase trapping on permeability reduction in an ultra-deep tight sandstone gas reservoirs

Dujie Zhang^{a,b,*}, Yili Kang^{a,**}, A.P.S. Selvadurai^b, Lijun You^a, Jian Tian^a

^a State Key Laboratory of Oil and Gas Reservoir Geology and Exploitation, Southwest Petroleum University, Chengdu, 610500, PR China

^b Department of Civil Engineering and Applied Mechanics, McGill University, Montréal, QC, H3A 0C3, Canada

ARTICLE INFO

Keywords:

Ultra-deep tight gas reservoirs
Phase trapping damage
Drill-in fluids
Invasion depth
Permeability damage ratio
Numerical simulation model

ABSTRACT

As the first external liquids that are introduced into a reservoir rock, suitable drill-in fluids not only prevent phase trapping-induced permeability reduction (also referred to as phase trapping damage) caused by the drill-in fluid itself but also minimize any phase trapping damage caused by the invasion of subsequent working fluids. An ultra-deep tight sandstone reservoir in the Tarim Basin, NW China is considered as a case study, and this paper presents the results of an extensive series of phase trapping damage investigations that were carried out to determine the permeability reduction in the reservoir rock that comes into contact with different working fluids during the processes of drilling, drill stem tests, completion and well tests. Both the pore microstructure and surface properties were also investigated. The experimental results showed that the integrated phase trapping damage ratio (*PDR*) of water-based drill-in fluids (WBDF)-organic salt completion fluids (*PDR* = 0.99) was greater than that of oil-based drill-in fluids (OBDF)-organic salt completion fluids (*PDR* = 0.88). The analysis suggests that the OBDF is more effectively in inhibiting the absorption of the filtrate of the completion fluids compared with WBDF. A procedure for reducing phase trapping damage by OBDF is presented, and a numerical simulation model is developed to validate the procedure. The results could be useful in understanding and selecting the best drill-in fluids and completion fluids to minimize phase trapping damage in ultra-deep tight gas reservoirs.

1. Introduction

Phase trapping refers to either the temporary or permanent trapping of oil- or water-based fluids introduced into a porous medium during drilling, completion and production operations (Bennion et al., 1999). The phase trapping-induced permeability reduction (also referred to as phase trapping damage) has a major influence on the performance of tight oil and gas reservoirs, and it has long been considered as one of the most severe formation damage mechanisms in tight gas reservoirs (Davis and Wood, 2004; Bennion et al., 2006). Damage occurs when the wetting phase, either water-based, hydrocarbon-based or gas-based, comes into contact with a sub-irreducibly saturated formation and is absorbed into the porous medium, reducing the relative permeability of the oil or gas (Fig. 1) (Bennion et al., 1996a; Saboorian-Jooybari and Pourafshary, 2017).

Evaluating phase trapping-induced permeability reduction in tight gas reservoirs has always been a problem of concern. You and Kang (2009) introduced the operational processes of aqueous phase trapping

damage experiment in detail. Bahrami et al. (2012a) performed laboratory experiments on West Australian core samples to compare the permeability damage caused by water/oil invasion, and the results indicated that the permeability was reduced up to 55% with oil invasion and up to 70% by water invasion. Ahmed Lashari et al. (2013) examined the change in permeability of a tight sandstone core after brine invasion, and showed that the permeability reduced to 20% of the initial value. Zhou et al. (2016) reported that the matrix permeability of a shale sample was altered and reduced by imbibition of fracturing fluids, and the reduction in some case reached as much as 95% based on the original permeability. Furthermore, a newly designed simulation of a three-step coreflood sequence, fracturing fluids-fluids invasion, flow-back and hydrocarbon production, was conducted by Longoria et al. (2017), who observed a significant reduction in permeability of an ultralow permeability core. Understanding the factors that influences phase trapping-induced permeability reduction is considered to be an important first step towards minimizing phase trapping damage. Previous studies suggest that the factors influencing phase trapping

* Corresponding author. State Key Laboratory of Oil and Gas Reservoir Geology and Exploitation, Southwest Petroleum University, Chengdu, 610500, PR China.

** Corresponding author.

E-mail addresses: dujie.zhang@mail.mcgill.ca (D. Zhang), cwct_fdc@163.com (Y. Kang).

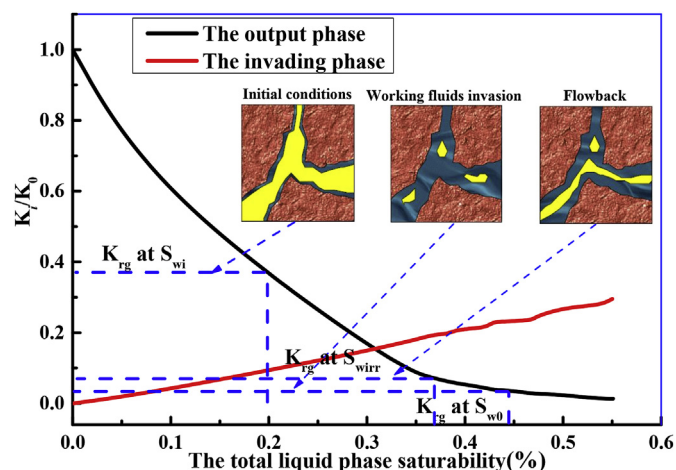


Fig. 1. Relative permeability curves of tight sandstone gas reservoirs considering phase trapping damage.

damage can include rock mineralogy, pore geometry, the tortuosity and the surface area of pores, wettability, interfacial tension (IFT), relative permeability, initial fluid saturation, the viscosity of the invading phase, microfractures, invasion depth, formation temperature, reservoir pressure and drawdown potential (Adams and Gast, 1997; Jerauld and Salter, 1990; Bennion et al., 1996b, 1999; Mirzaei-Paiaman et al., 2011; Bahrami et al., 2012b; Cai et al., 2014; Yang et al., 2016; Zhang et al., 2019). Based on these observations, many control methods have been proposed to prevent phase trapping damage and the optimization of the drill-in fluid system is considered as the most effective approach, which can include the selection of optimum properties of drill-in fluids that can minimize the invasion depth of working fluids. As the first external liquid comes into contact with the reservoir formation, the anti-phase-trapping-damage properties of drill-in fluids are critical. Suitable drill-in fluids not only prevent phase trapping damage caused by the drill-in fluid itself but also minimize the phase trapping damage caused by subsequent working fluids. Therefore, understanding the phase trapping damage mechanisms induced by drill-in fluid systems is an essential first step. Bahrami et al. (2012a) reported that an oil-based drill-in fluid (OBDF) can reduce the phase trapping damage of West Australian tight gas reservoirs compared with water-based drill-in fluids (WBDF). Ahmed Lashari et al. (2013) also indicated that Malaysian diesel-oil-based drill-in fluids could minimize the phase trapping damage of low permeability and tight cores. Although the conclusions were similar, the evaluation results from other tight sandstones indicated differences due to the rock composition and the working fluid properties.

For ultra-deep tight sandstone gas reservoirs, the geological conditions are more severe and the types of working fluids used are more complex compared with conventional tight gas reservoirs. Since ultra-

deep gas fields are in the early stages of development, documentation is scarce. There is no consensus on a drill-in fluid system selection process to minimize phase trapping damage. For example, in the ultra-deep tight sandstone gas reservoir in the K9 gas field of the Tarim Basin, NW China, both WBDF and OBDF were used simultaneously. It is not clear which is more appropriate. Therefore, this research focused on a series of experiments to help select the best drill-in fluids to minimize phase trapping damage in this reservoir. First, the geological setting was introduced, and an experimental technique was then developed to evaluate the phase trapping damage caused by formation water and a diesel oil (Chinese # 0 diesel oil). In addition, a novel method was developed to evaluate the integrated phase trapping damage induced by drill-in fluids and completion fluids, taking into account the processes of drilling, drill stem tests, completion and well tests. The pore microstructure and surface properties were analyzed based on the results of X-ray diffraction (XRD), Scanning Electron Microscopy (SEM), Mercury Injection Capillary Pressure tests (MICP), low-temperature nitrogen adsorption experiments and Nuclear Magnetic Resonance tests (NMR) to interpret the results. In addition, a procedure for reducing phase trapping damage by OBDF is presented. Finally, a computational model was developed to examine the influence of the invasion depth of completion fluids on the gas extraction capacity from the matrix to the fracture under constant production pressure. This work will be beneficial for the precise assessment of the phase trapping damage and optimization of the drill-in fluid system for ultra-deep tight sandstone gas reservoirs.

2. Geological setting

The K9 gas reservoir is in the Kelasu structure belt located on the north side of the Kuqa depression, in the northern section of the Tarim Basin (Fig. 2). The depth of the main pay zone is 6500 m–8000 m, and the maximum effective thickness of the pay zone is 150 m (Graham et al., 1993; Zou et al., 2012; Selvadurai et al., 2018). The proven gas reserves are estimated to be $5485 \times 10^8 \text{ m}^3$. The reservoir is under the combined influences of diagenetic compaction and tectonic compression. The main sedimentary facies are braided river deposits. The reservoir sandstones consist mostly of lithic arkose sandstone and feldspar lithic sandstone. The maturity grade of the rock structure and contents are low; the lithic fragment content ranges from 18%–22%, and 19.4% on average. The filling in the sandstone reservoir includes silica and calcareous cement. The porosity is 2%–7%, and the permeability is approximately 0.001 mD to 0.5 mD. Due to three stages of tectonic evolution and the specific tectonic stress, the natural fractures are well developed. The linear density of the natural fractures is between 0.7 stripe/m and 1.47 stripe/m based on the well log data (Feng et al., 2018). The formation pressure coefficient of this reservoir ranges from 1.75 to 1.80, and the geothermal gradient of the reservoir is $2.19 \text{ }^\circ\text{C}/100 \text{ m}$ – $2.30 \text{ }^\circ\text{C}/100 \text{ m}$. The total salinity of the formation water reaches 200 000 mg/L. Many of the exploration wells, including those that have

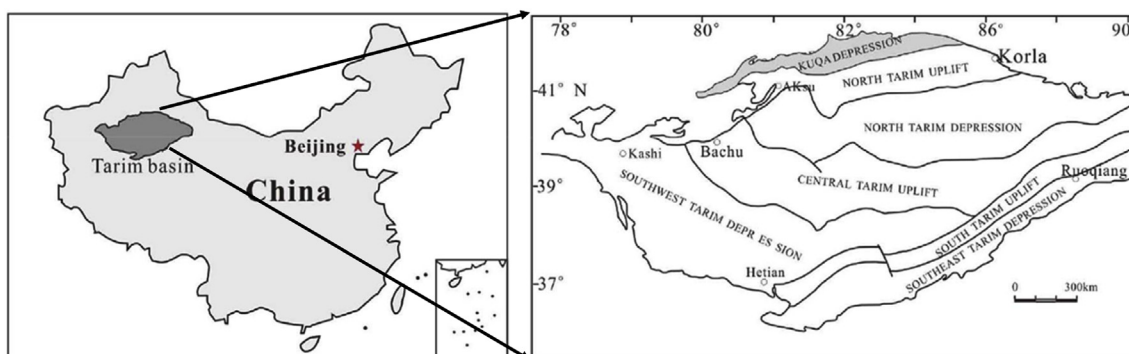


Fig. 2. Structure of the Kelasu structural belt in the Kuqa depression (Lai et al., 2018).

Table 1
Buried depth and physical parameters of the rock samples.

Cores	Depth (m)	Length (mm)	Diameter (mm)	Porosity (%)	K (mD)
KS2-9	7973.81	30.50	25.40	2.05	0.00410
KS1-6	7730.95	50.10	25.40	4.38	0.00875
KS1-7	7733.53	51.01	25.40	5.86	0.01550
KS1-17	7851.94	52.33	25.40	2.41	0.01936
KS3-5	7852.91	49.99	25.40	2.94	0.01879
KS3-4	7899.05	46.52	25.40	1.72	0.03349
KS3-9	7907.43	54.38	25.40	1.93	0.02081
KS3-1	7892.94	53.14	25.40	2.43	0.03337
KS3-7	7903.56	50.10	25.40	2.55	0.02536

been drilled into the deeply buried structures have yielded a high well production of natural gas, which indicates that the Bashijiqike sandstones are highly productive even at these deep burial depths (> 7000 m).

3. Materials and experimental methods

3.1. Materials

Several fresh tight sandstone samples were collected from the ultra-deep sandstone gas reservoir in the K9 gas field, at a depth of over 7500 m. Cylindrical samples with a diameter of 2.540 cm and length of 3 cm–6 cm were used for the experiments; detailed information is given in Table 1. Prior to the experiments, the rock samples were dried in incubators maintained at a temperature of 60 °C for up to 48 h until no further weight change occurred.

The formation water was prepared based on an elemental analysis of the production formation water as shown in Table 2, and the inorganic salts used were analytical reagents. The OBDF base oil was Chinese # 0 diesel oil. The OBDF, WBDF, and water-based completion fluids were collected from the K9 gas field, and the filtrate of the working fluids used for the experiments was collected at a positive pressure of 3.5 MPa.

3.2. Experiments

3.2.1. Comprehensive phase trapping damage tests

There are many kinds of working fluids present in the reservoirs during gas exploration, including drill-in fluids and completion fluids. Due to the different characteristics of the working fluids, the amount of the working fluid inflow and outflow could influence the degree of phase trapping damage. To the authors' knowledge, there have been no studies to date that have focused on this aspect. Therefore, a new experimental procedure was designed to evaluate the phase trapping damage induced by the sequential contact of the host rock with the working fluids. A schematic diagram for coreflood experimental apparatus is shown in Fig. 3. The process of drilling, the drill stem tests (DST), the well completion and the well tests were simulated; the experimental processes included filtrate imbibition of drill-in fluids, a first flowback test, the filtrate imbibition of completion fluids and a second flowback test, as shown in Fig. 4. In order to ensure the consistency of the experiments in this study and to simplify the experimental procedure, only organic salt completion fluids were used.

The detailed experimental steps are as follows: ① Ultra-tight

Table 2
Elemental analysis of the formation water.

Inorganic salt types	NaHCO ₃	Na ₂ SO ₄	NaCl	MgCl ₂	CaCl ₂	Total salinity
Content (mg/L)	243.6	604.9	171 497.0	3744.0	28 837.8	204 927.3

sandstone samples were cleaned with methanol using a vacuum extractor, and the weight, permeability, and porosity were measured. ② Initial water saturation was established using formation water, and the initial gas permeability was measured under the initial water saturation, K_0 . ③ The spontaneous imbibition experiment with the filtrate of drill-in fluids was conducted, and the imbibition weight of the filtrate was recorded automatically on a computer; the experimental run time was set to 16 h ④ Nitrogen was used to flood the sample from the opposite direction of spontaneous imbibition, and the weight of the sample was measured every hour to determine the residual liquid saturation, with a positive pressure gradient of 0.5 MPa/cm; the experimental run time was set to 7 h ⑤ The ultimate permeability K_d was measured after the flowback process, and the phase trapping damage ratio, defined by $PDR_d = [1 - (K_d/K_0)]$ was estimated. ⑥ Completion fluids were used to repeat steps ③, ④ and ⑤, and the integrated phase trapping damage ratio, defined by $PDR_t = [1 - (K_t/K_0)]$, was calculated. The degree of phase trapping damage can be classified into different levels based on the guidelines given in Table 3 (You and Kang, 2009). High-pressure nitrogen was used to provide inlet pressure (p_{int}) to simulate the constant production pressure. The outlet pressure p_{out} was set to 0.9 MPa to eliminate the gas slippage effect (You et al., 2013). Confining pressure (p_{con}) was controlled by a constant pressure system, and the net confining pressure ($p_{net} = p_{con} - (p_{int} + p_{out})/2$) was set to 3 MPa. The two ends of the core are fixed boundaries. For comparison, the WBDF was also evaluated; the experimental stages of WBDF and OBDF were similar except for the first spontaneous imbibition liquid.

3.2.2. Measurement of aqueous phase retention

Understanding liquid phase retention can assist in controlling phase trapping damage. In this study, Nuclear Magnetic Resonance tests (NMR) was used as a non-destructive technique to characterize the aqueous phase retention in the tight sandstone cores (Li et al., 2018). The apparatus used was the full diameter core NMR analysis system (AniMR-150), and the diameter of the experimental cores varied between 25 mm and 125 mm. According to the theoretical basis of the NMR, the position and volume of the water in pores can be indicated through the T_2 relaxation time of the test sample, which was recorded. For better comparison, the same sample was measured after saturation, absorption and flowback experiments, and the saturated sample treated as the control sample. The sample was then cleaned, and the imbibition and displacement processes were consistent with the steps of the comprehensive phase trapping damage experiments.

3.2.3. Characterization of the pore microstructure and surface properties

The pore and clay mineral structures were observed using a scanning electron microscope (SEM) (Quanta 250, FEI), and the test accuracy ranged from 100 nm to 3500 μ m. A high-pressure mercury porosimeter (AutoPore IV 9505) was selected to measure the pore size distribution of the samples. The device can measure pore sizes from 0.1 nm to 1000 μ m, with a maximum mercury injection pressure of 228 MPa.

Low-temperature (77 K) N₂ adsorption was used to accurately describe the pores sizes, which ranged from 0.35 nm to 200 nm; the equipment used a NOVA2000e analyzer (Quantachrome Instruments). The pore size distribution and related pore shapes were determined by analyzing the nitrogen adsorption/desorption isotherms.

The wettability of the samples was evaluated by contact angle measurements performed with an optical contact angle measurement instrument (DSA100, KRUS) using a plate-like sample. The range of contact angles that could be measured was 0°–180°, and the measurement resolution was $\pm 0.1^\circ$.

The Interfacial tension (IFT) values between the filtrate of drill-in fluids and nitrogen were measured using the modified TX-500D spinning drop interface tension meter. All measurements were conducted at room temperature (25 °C) with a constant rotation of 6000 rpm until the IFT did not change.

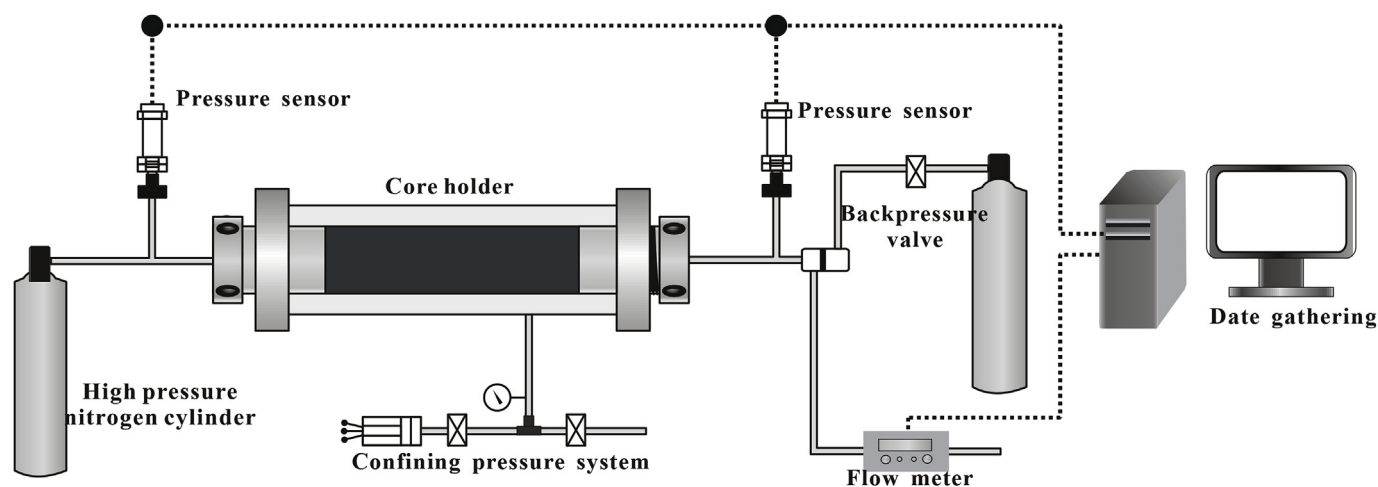


Fig. 3. Schematic view of the coreflood experiment.

4. Results and discussion

4.1. Results of aqueous/hydrocarbon phase trapping damage

Fig. 5(a) shows the change in the liquid saturation during the imbibition process of both aqueous and hydrocarbon phase trapping damage experiments. The liquid saturation curves of KS1-6 and KS1-7 are generally higher than those of KS1-17 and KS3-5. The analysis shows that the liquid saturation curves of KS1-6 and KS1-7 appear to be divided into two stages: a rapidly rising stage and a stable stage. The rapidly rising stage lasted almost 2 h before the start of the stable stage. In the rapidly rising stage, the aqueous saturation increased up about 90% of the total liquid saturation. The imbibition curves of KS1-17 and KS3-5 displayed a different trend; there was no rapid increase in the curves similar to those of KS1-6 and KS1-7, and the imbibition rate remained steady over the remaining hours. In order to clearly understand the imbibition channels of the aqueous and the hydrocarbon phase, the relationship between the liquid saturation and the square root of imbibition time were plotted as shown in Fig. 5(b). It can be seen that the imbibition of formation water occurred in two separate phases, and their slopes for saturation vs. time varied widely. The slope of phase 2 was considerably smaller than that of phase 1. The imbibition rate of formation water during phase 1 was much faster than during phase 2. Based on previous analysis (Roychaudhuri et al., 2013), the imbibition channels during phase 1 and phase 2 were identified as the micro-fracture network and the matrix, respectively. However, the imbibition of hydrocarbon occurred only in a single phase, and the imbibition rate was nearly linear with respect to the square root of time. Hence, the micro-fractures were considered to be the main hydrocarbon imbibition channel. The average slope of the hydrocarbon imbibition curves was significantly less than that of phase 1 of the formation water imbibition curves. Therefore, reducing the contact time between hydrocarbon-based working fluids and the reservoir formation is likely to reduce the imbibition volume compared with water-based working fluids.

As shown in Table 4, the average flowback rate of hydrocarbon was 48.63%, which was higher than that of the aqueous phase (26.48%).

Since the main imbibition channels for hydrocarbon were micro-fractures, the diesel oil was more easily displaced. Meanwhile, the average PDR of hydrocarbon was 0.54, and the degree of phase trapping damage was medium. The average PDR of the aqueous phase was 0.75, and the degree of phase trapping damage was clarified as intense. The phase trapping damage induced by diesel oil was less than for the formation water. Thus, it can be concluded that OBDF is better at preventing phase trapping damage compared to WBDF.

4.2. Comparison of phase trapping damage induced by working fluids

During the first imbibition and flowback processes, the OBDF and WBDF were used as the imbibition fluids, and the experimental cores were KS3-4, KS3-9, KS3-1 and KS3-7. The initial water saturation of KS3-4, KS3-9, KS3-1 and KS3-7, was set to 22.65%, 20.91%, 21.97% and 21.28%, respectively. Fig. 6 shows the liquid saturation change during the first imbibition and flowback processes. As shown in Fig. 6(a), the liquid saturation of the samples increased with imbibition time in the first imbibition process. The saturation curves of KS3-4, KS3-9, KS3-1 and KS3-7 showed the same trend as that of formation water and diesel oil shown in Fig. 5(a). Based on these experimental results, the total liquid saturation of KS3-1 and KS3-7 was larger than that of KS3-4 and KS3-9, which indicates that the filtrate of WBDF was more easily imbibed than the OBDF. The liquid saturation change curves of the first flowback process are shown in Fig. 6(b). The saturation reduction rate for the WBDF was slightly greater than that of the OBDF.

As shown in Fig. 6, the final liquid saturation of KS3-1 and KS3-7 was far above KS3-4 and KS3-9, which indicates that the entrapment volume of OBDF filtrate was smaller than that of WBDF. As shown in Table 5, the average PDR of KS3-4 and KS3-9 was 0.61, which was smaller than for KS3-1 and KS3-7 (0.78 on average). These results illustrate that even though the residual invading oil filtrate resulted in the entrapment of an additional third phase (Bahrami et al., 2012a), OBDF was still more beneficial in reducing phase trapping damage compared to WBDF.

The second imbibition-flowback process investigated the effect of

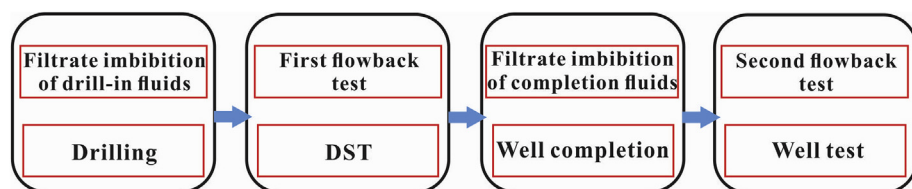


Fig. 4. The experiment procedures for the evaluation processes.

Table 3
Interpretation criteria for calculated values of phase trapping damage ratio.

Range	$PDR < 0.05$	$0.05 \leq PDR < 0.3$	$0.3 \leq PDR < 0.7$	$0.7 \leq PDR < 1$
Damage-potential severity	None	Weak	Medium	Intense

different drill-in fluids on the phase trapping damage induced by the subsequent completion fluid. During these processes, the organic salt completion fluids were used as the imbibition fluids, and the experimental samples used were KS3-4, KS3-9, KS3-1 and KS3-7 after imbibition of either OBDF or WBDF. Fig. 7 displays the liquid saturation change during the second imbibition-flowback process. As shown in Fig. 7(a), there was only a slight increase of in the total liquid saturation level for KS3-4 and KS3-9, which were previously treated by OBDF, and the time for this increase was mainly in the first two hours, with only a small increase thereafter. For KS3-1 and KS3-7, previously treated by WBDF, the increase in liquid saturation also mainly occurred in the first ten hours, but the final fluid saturation was much larger than for KS3-4 and KS3-9. These experimental results demonstrate that an OBDF appears to inhibit subsequent invasion of organic salt completion fluids. The liquid saturation curves during the coreflood process are shown in Fig. 7(b). The total liquid saturation of the samples decreased during the coreflood process, and the residual liquid saturation of KS3-1 and KS3-7 was much larger than KS3-4 and KS3-9.

Based on the results of the experiments, it can be seen that OBDF reduced the imbibition volume during the subsequent use of water-based completion fluids. According to the calculated *PDR* as shown in Table 6, the *PDR* of KS3-4, KS3-9, KS3-1 and KS3-7 were 0.86, 0.89, 0.99 and 0.98, respectively. In other words, the residual filtrate of OBDF played a role in reducing the phase trapping damage during the second imbibition-flowback process.

4.3. Factors influencing extensive phase trapping damage

4.3.1. Complex pore throat structure

In the reservoir rock used in these experiments, X-Ray Diffraction analysis shows that the main clay minerals are illite (59.42%), chlorite (24.72%) and illite/smectite inter-stratified clay mineral (15.86%). As shown in Fig. 8, SEM images display many dense vertical fibres of illite between the rock grains and micro-fractures. The clay minerals divide the seepage space into much smaller channels, thus causing a higher capillary force for any wetting phase. As a result, the wetting phase is

more easily absorbed deeply into the reservoir and is harder to displace (Mahadevan et al., 2007; Ghanbari and Dehghanpour, 2015). In addition, the illite/smectite inter-stratified clay mineral typically has a high specific surface area with strong water absorption ability. These clay minerals can absorb a significantly greater volume of water and cause wetting phase retention (Liu et al., 2016).

The capillary pressures of the tight sandstone samples were measured by a Mercury Injection Capillary Pressure test (MICP), and the intrusion-extrusion curves are shown in Fig. 9. Based on the assumption of cylindrical pores, the pore size distribution can be calculated by the Washburn equation (Yao and Liu, 2012): $R_c = (-2\sigma \cos \theta)/P_c$, where P_c is the absolute injection pressure, R_c is the pore radius (μm) when mercury enters at the pressure P_c (MPa); θ is the contact angle between mercury and the pore surface; and σ is the interfacial tension of mercury. Therefore, it is not difficult to see that if the injection curve has a steep slope and a very small flat section, only a small proportion of the pores have the same diameter, thus the steeper the slope and the smaller the flat section, the smaller the proportion of pores with the same diameter is, i.e. intense heterogeneity of the pore-throat size. As shown in Fig. 9, the curves have a steep slope with a very small flat section in the mercury injection curves, which indicates that the heterogeneity of the pore-throat size was dominant. Table 7 shows that the threshold pressure of this reservoir rock ranges from 1.14 MPa to 8.90 MPa, with an average of 5.11 MPa. The median saturation pressure ranges from 40.93 MPa to 92.30 MPa, with an average of 66.29 MPa. The average pore throat radius ranges from 0.0145 μm to 0.0850 μm , with an average of 0.0324 μm . Furthermore, about 62.52% of the injected mercury remains within the sample at the end of the extrusion. From these results we can deduce that the pore geometries are comprised of a system of large body pores but interconnected by very narrow throats, and the differences in the pore and throat sizes are considerable. Based on the experimental results of MICP tests, this reservoir rock can be characterized as having narrow pore and pore-throat sizes, strong heterogeneity of throat size and complex pore geometries. According to the mechanisms of liquid phase trapping damage (You and Kang, 2009), these features would aggravate the

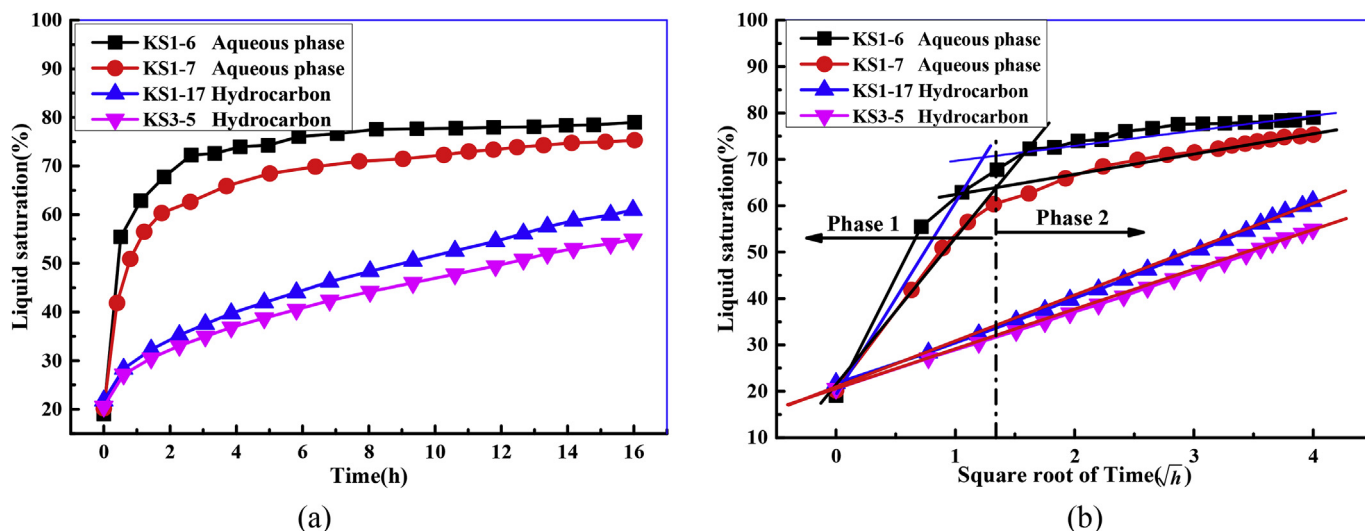


Fig. 5. (a) Liquid saturation curves of aqueous/hydrocarbon phase trapping damage during the imbibition process, (b) Relationship between saturation and the square root of imbibition time of aqueous/hydrocarbon phase trapping damage during the imbibition process.

Table 4
Results of the imbibition/flowback processes of phase trapping damage experiments.

Cores	Initial water Saturation (%)	K_{wi} (mD)	Imbibition volume (PV)	Flowback volume (PV)	Flowback rate (%)	PDR	Fluid type
KS1-6	19.06	0.001240	0.600	0.161	26.83	0.73	Formation water
KS1-7	20.18	0.002650	0.551	0.144	26.13	0.76	
KS1-17	21.76	0.006730	0.392	0.175	44.64	0.52	# 0 diesel oil
KS3-5	20.55	0.004102	0.344	0.181	52.62	0.55	

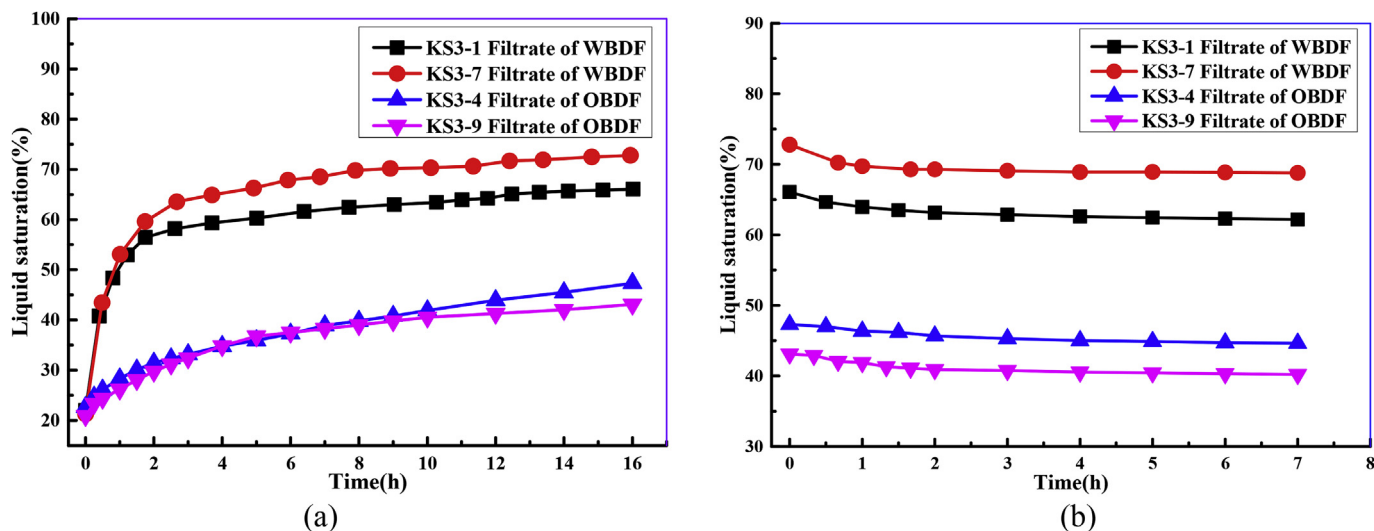


Fig. 6. Imbibition-flowback curves of the first imbibition-flowback process. (a) imbibition process; (b) flowback process.

Table 5
Results of the first imbibition-flowback process.

Cores	Initial water Saturation (%)	K_{wi} (mD)	Imbibition Volume (PV)	Flowback Volume (PV)	Flowback rate (%)	PDR	Fluid type
KS3-4	22.65	0.001899	0.247	0.027	10.93	0.63	OBDF
KS3-9	20.91	0.001669	0.222	0.029	13.06	0.58	
KS3-1	21.97	0.002161	0.441	0.039	8.84	0.82	WBDF
KS3-7	21.28	0.001994	0.515	0.040	7.77	0.74	

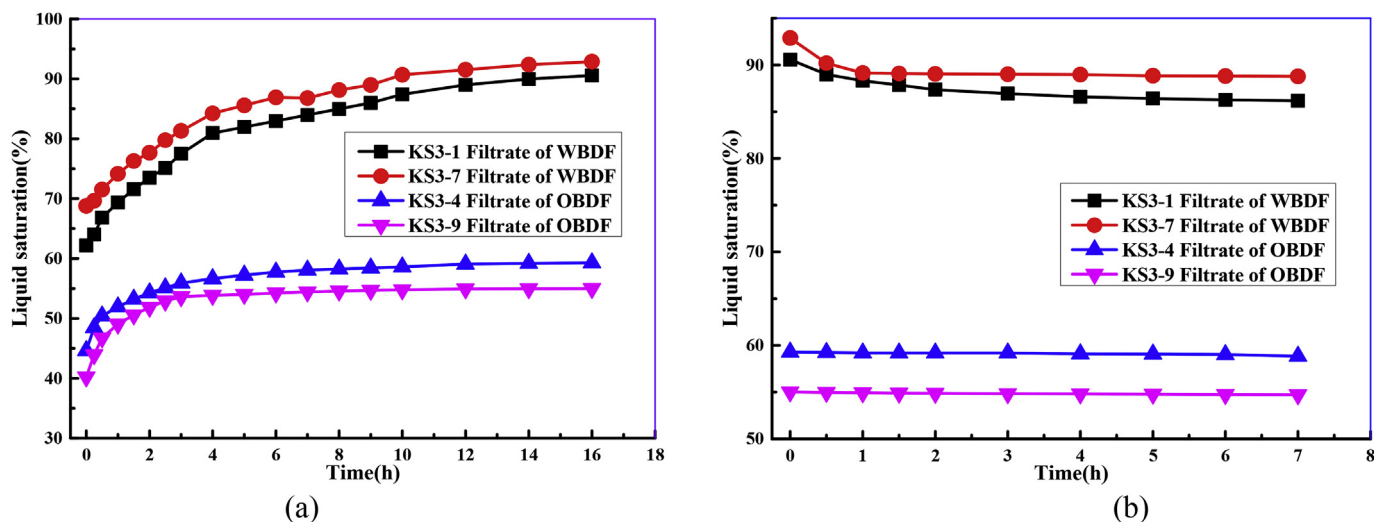


Fig. 7. Liquid saturation curves of the second imbibition-flowback process. (a) imbibition process; (b) flowback process.

invasion and retention of the wetting fluid and reduce the flowback rate; this would exacerbate the degree of phase trapping damage in the ultra-deep tight sandstone gas reservoirs.

In order to further determine the microscopic pore structure, a

nitrogen adsorption experiment was carried out. As indicated in Fig. 10, the nitrogen isotherms show that the adsorption/desorption processes of the samples were not reversible due to hysteresis (Labani et al., 2013). According to the classifications of adsorption isotherms shown

Table 6
Results of the second imbibition-flowback process.

Cores	K_{wi} (mD)	Imbibition volume (PV)	Flowback volume (PV)	Flowback rate (%)	PDR	Fluid type
KS3-4	0.001899	0.146	0.004	2.74	0.86	Organic salt
KS3-9	0.001669	0.148	0.003	2.03	0.89	completion
KS3-1	0.002161	0.284	0.044	15.49	0.99	fluids
KS3-7	0.001994	0.241	0.041	17.01	0.98	

in Fig. 11(a) (Brunauer et al., 1940), Type II isotherms are used to analyze the pore structure of the samples based on the shapes of these curves. In general, Type II isotherms could be interpreted as the filling of the micropore at low relative pressures, and, due to the presence of macropores in the samples, the adsorption isotherm rises rapidly when $P/P_0 = 1$, where P is the gas vapor pressure in the system and P_0 is the saturation pressure of the adsorbent. The amount of adsorbed gas at low relative pressures reflects the volume of the micropore and fine mesopores.

In addition, the hysteresis loop is characterized by desorption shoulders and lower closure points. Based on the four types of hysteresis loops identified by IUPAC, H1 - H4, as show in Fig. 11(b) (Sing and Williams, 2004), the Type H1 hysteresis loop can be attributed to adsorbents with a narrow distribution of uniform pores (open-ended tubular pores). The Type H2 hysteresis loop can be attributed to complex pore structures, which are characterized by an interconnected network of pores of different sizes and shapes. The Type H3 hysteresis loop is usually obtained from aggregates of plate-like particles or adsorbents containing slit-shaped pores. The Type H4 hysteresis loops are also formed by slit-shaped pores and are characteristic of activated carbons. The hysteresis loops with the H3 and H4 shapes often do not close until the pressure is at, or very close to, the saturation pressure. The morphological features identified from our experiments indicated that the type of hysteresis loop observed was Type H3. Therefore, we can speculate that the main pores in this reservoir were slit-shaped.

The pore size distribution calculated from nitrogen adsorption experiments is shown in Fig. 12. The results indicate that the pore structure of the samples is characterized by one peak, and the radius of the main pores ranged from 2 nm to 10 nm.

By combining the results of SEM, MICP and nitrogen adsorption experiments, it can be concluded that this reservoir is characterized by hair-like and silk-thread clays in flaky seepage channels, with curved lamellar throats, developed micro pores and nanoscale pores, which promotes absorption and inhibits the flowback of the wetting phase. This results in severe phase trapping damage. On basis of the laboratory experiments, the contact angle of formation water and Chinese # 0

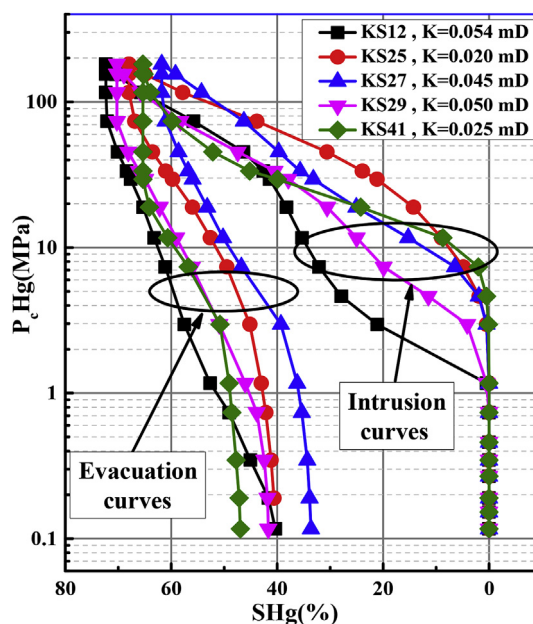


Fig. 9. Intrusion and extrusion curves for five samples obtained from the MICP test.

diesel oil against this reservoir rock are 44.6° and 66.8°, respectively, which indicates that this reservoir is oil/water wet. If either water-based drill-in fluids (WBDF) or OBDP are used in this reservoir, the filtrate of working fluids will invade the reservoir and result in phase trapping damage.

4.3.2. Abnormal low initial water saturation

The permeability at irreducible water saturation (S_{wirr}) is usually far less than that under initial water saturation. Therefore, the difference between the initial water saturation and irreducible water saturation is very important to phase trapping damage. According to the well-log interpretation as shown in Fig. 13, the initial water saturation of this reservoir was on average 23.7%. The irreducible water saturation of this reservoir was 39.36%, which was evaluated at 160 °C and 116 MPa pore pressure (Fang et al., 2015). The large difference between the initial water saturation and the irreducible water indicates that this reservoir can easily suffer severe aqueous phase trapping damage.

4.3.3. Distribution of the retained aqueous phase

As shown in Fig. 14, the T_2 response curves of the same rock samples after saturation, absorption and flowback experiments are plotted.

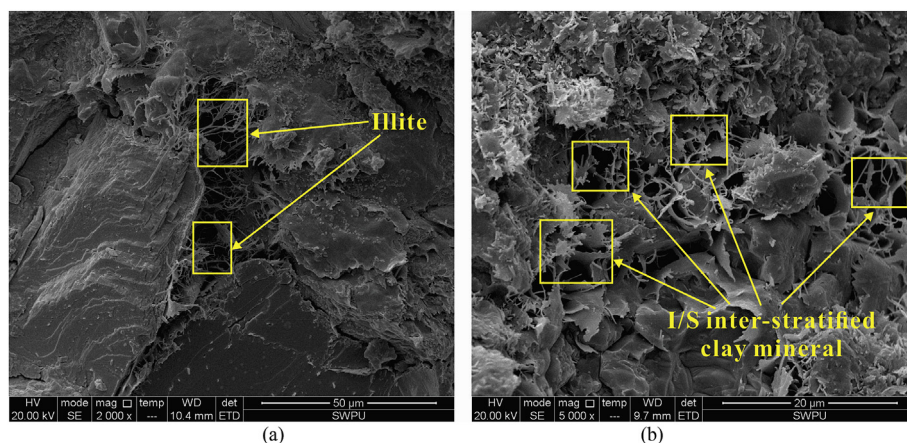


Fig. 8. SEM images of the tight sandstone samples. (a) illite. (b) illite/smectite interstratified clay mineral.

Table 7
Parameters of pore throat structure of five samples using the MICP test.

Cores	Threshold Pressure (MPa)	Median saturation Pressure (MPa)	Average radius (μm)	Uniformity coefficients	Sorting coefficient	Efficiency of mercury withdrawal (%)
KS12	1.14	56.52	0.0850	0.0933	1.4465	44.22
KS25	7.56	90.76	0.0145	0.0918	2.8594	40.74
KS27	5.49	92.30	0.0249	0.1066	2.5541	33.63
KS29	2.46	50.96	0.0147	0.0917	2.5682	40.67
KS41	8.90	40.93	0.0228	0.1651	2.1029	28.16

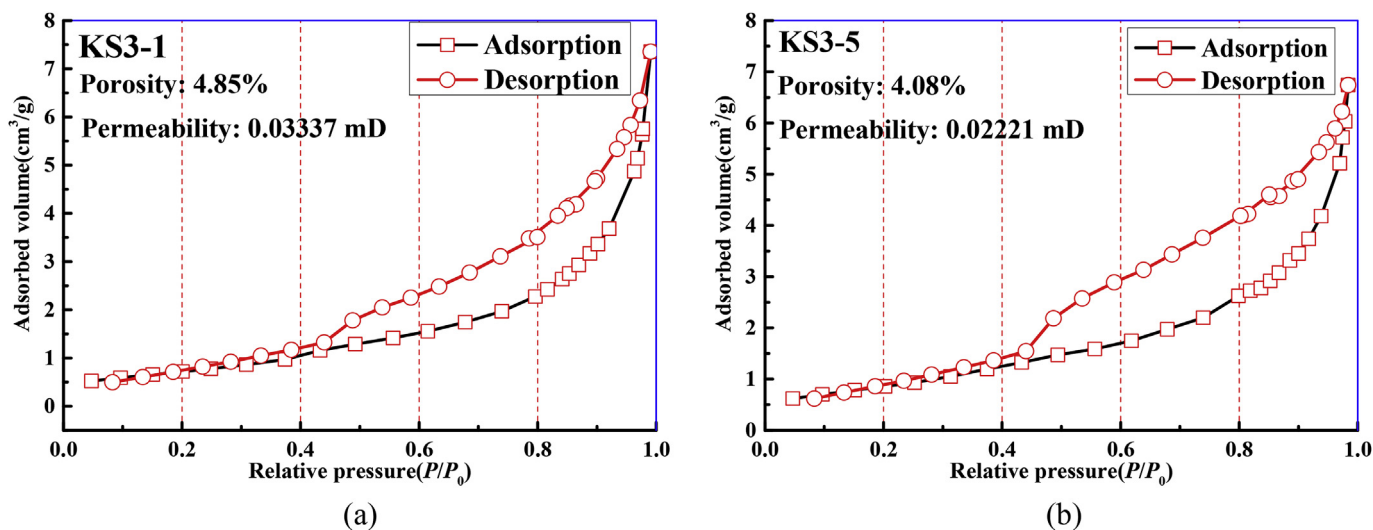


Fig. 10. Adsorption/desorption isotherms. (a) KS3-1 and (b) KS3-5.

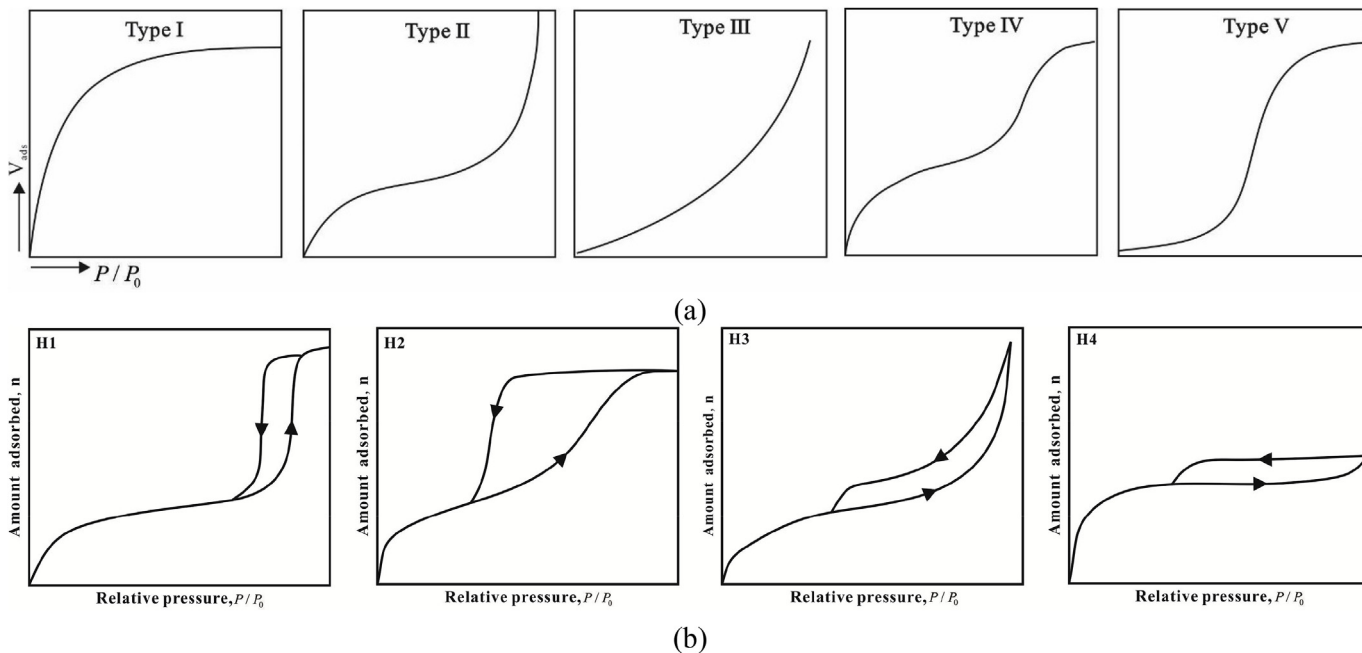


Fig. 11. (a) Adsorption isotherm types (Brunauer et al., 1940), (b) The four types of hysteresis loops identified by IUPAC (Sing and Williams, 2004).

The working fluid is formation water. The results indicate that there are two isolated peaks in the T_2 response curves of the sandstone rock samples after the treatments. The left peak is in the section between 0.01 ms and 10 ms, and occupies a large part of the total spectrum area. The right peak is in the section between 10 ms and 600 ms, and only occupies a smaller part of the spectrum area. The maximum value of the saturated curve is close to 600 ms, but the maximum value of the

absorption curve is only 200 ms. The pore volume represented by the difference is known as the defect in the rocky surface. According to the tendency of the curves, the spectrum area of the sample after saturation, absorption and flowback experiments is a gradual degradation, and the reduction percentage of the left peak is smaller than the right peak. These results indicate that it is difficult to displace the formation water filling the relatively narrower pores. In other words, most of the

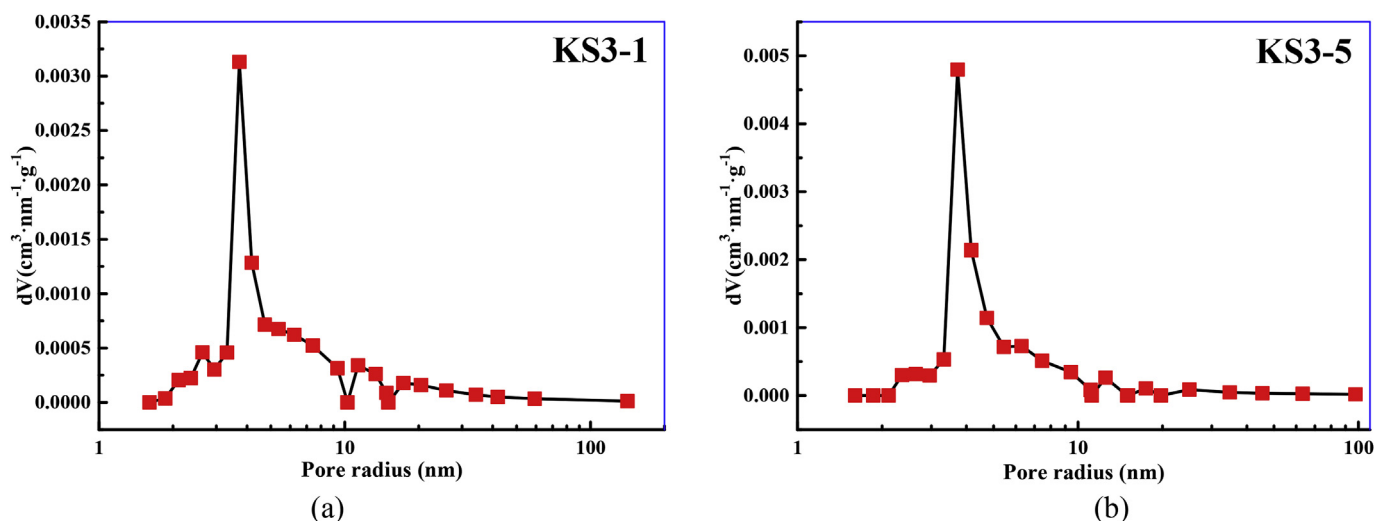


Fig. 12. Pore size distribution of two samples according to the desorption isotherms: (a) Pore size distribution of KS3-1, (b) Pore size distribution of KS3-5.

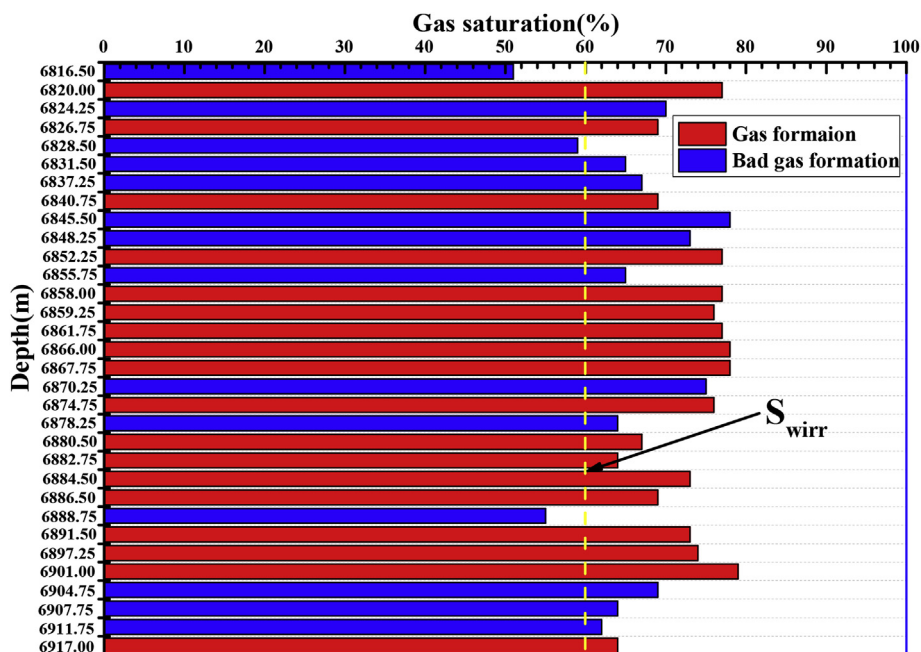


Fig. 13. Initial gas saturation of tight gas reservoirs based on well-log interpretation.

invading fluids will be retained in the pores, resulting in serious phase trapping damage.

4.4. Mechanisms to reduce phase trapping damage by OBDF

4.4.1. The bigger contact angle and the smaller IFT

Based on the results of the repeated imbibition-flowback experiments, it was found that OBDF reduces phase trapping damage compared to WBDF. In general, it is believed that the contact angle and IFT (Interfacial tension) are the most important factors influencing the degree of phase trapping damage. Based on the results of wettability measurements, the contact angle of the filtrate of WBDF against rock is about 23.2°, and that of the filtrate of OBDF against rock is about 66.8°. The filtrate of WBDF shows a stronger wettability compared with OBDF, and the trend of the imbibition curves agree with the experimental results. Thus, the invasion filtrate volume of WBDF should be larger than that of OBDF. Furthermore, according to the results of the IFT measurements, the IFT of the filtrate of OBDF and WBDF were

23.51 mN/m and 63.46 mN/m, respectively. These results indicate that the filtrate of OBDF was more easily displaced by nitrogen than the filtrate of WBDF (Babadagli et al., 1999). Therefore, the filtrate of OBDF not only reduced the invasion filtrate volume but also increased the flowback rate.

4.4.2. Effect of the entrapment of an additional third phase

Based on the experimental results as shown in Table 6, OBDF reduces the phase trapping damage in the second imbibition-flowback process. The main mechanism was explained by the reduction of the imbibition volume of the completion fluids, so as to control the corresponding invasion depth. It was observed that there were some residual oil droplets remaining in the pore throat after the first flowback process. During the process of the second imbibition, the residual oil droplets play an important role, influencing the comprehensive phase trapping damage; a procedure to produce phase trapping damage by OBDF is shown schematically in Fig. 15. First, the residual oil droplets plug the seepage channels during the second imbibition process. As a

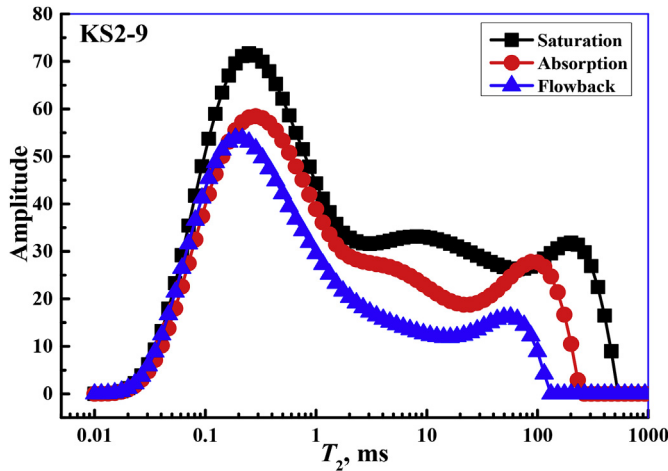


Fig. 14. NMR T_2 response curves of tight sandstone samples after saturation, absorption and flowback.

result, the imbibition volume for KS3-4 and KS3-9 is much less than for KS3-1 and KS3-7. Then, although the flowback rate in samples damaged by OBDP is smaller, there is only a small volume of invading fluid that remains in the second flowback process. Therefore, the damage range caused by the organic salt completion fluids does not penetrate as deeply. Even though the degree of damage in the three-phase seepage zone induced by the invasion of subsequent water-based working fluids is worse, the total damaged depth is shallower. If the depth of the three-phase seepage is shallow enough, even if the permeability damage ratio of the three-phase flow zone is large, the total phase trapping damage ratio will be much less than in the reservoir using WBDF and organic salt completion fluids.

4.4.3. Validation of the procedure for reducing phase trapping damage by OBDP

In order to verify the effectiveness of OBDP in reducing phase trapping damage, a test configuration was modelled using the finite element code COMSOL®. The simulated region measured 15 m in the horizontal direction and 2 m in the vertical direction. Equation (1) was used to model the gas production process from the damaged fracture face (Lie, 2014; Selvadurai, 2000; Selvadurai and Najari, 2015; Selvadurai and Suvorov, 2016).

$$(C_g + C_r)\varphi\rho_g \frac{\partial p}{\partial t} - \nabla \cdot \left(\frac{\rho_g K}{\mu} \nabla p \right) = Q_p \tag{1}$$

where p is the pore gas pressure (MPa), K is the permeability (mD), μ is the dynamic viscosity of the natural gas (Pa·s), φ is the porosity, C_g is the isothermal compressibility coefficient of the natural gas ($C_g = \partial\rho/(\rho\cdot\partial p)$, Pa⁻¹) C_r is the rock compressibility ($C_r = d\varphi/(\varphi\cdot dp)$, Pa⁻¹), ρ_g is gas density (g/cm³), Q_p is the source term.

Natural gas is very compressible, and the viscosity and compressibility will change considerably with changes in pressure. Therefore, the relationship between the compressibility of the natural gas and gas pressure was described as follow (Heidaryan et al., 2010):

$$C_g = \frac{1}{p} - \frac{1}{Z} \left(\frac{\partial Z}{\partial p} \right)_T \tag{2}$$

where Z is the compressibility factor. The Z -factor can be estimated with a developed correlation in terms of the pseudo-reduced pressure (p_r) and pseudo-reduced temperature (T_r) (Mahmoud, 2013)

$$Z = 0.702e^{-2.5T_r} p_r^2 - 5.524e^{-2.5T_r} p_r + (0.044T_r^2 - 0.164T_r + 1.15) \tag{3}$$

where $p_r = p/p_c$, $T_r = T/T_c$, and p_c and T_c are the critical pressure (4.59 MPa) and critical temperature (190.55 K) of methane, respectively. In this study, the reservoir temperature remains constant (433.15 K).

Gas viscosity can also be estimated using the following correlation (Lee et al., 1966):

$$\mu = 10^{-4} a e^{b\rho_g^c} \tag{4}$$

where μ is the gas viscosity (cp), $a = \frac{(9.379 + 0.01607M_g)T^{1.5}}{209.2 + 19.26M_g + T}$, $b = 3.448 + \left(\frac{986.4}{T}\right) + 0.01M_g$, $c = 2.447 - 0.2224b$, T is the Rankine temperature (°R).

Gas density can be estimated using the following correlation: $\rho_g = M_g P/ZRT$, where M_g is the molecular weight of the gas (16.0425 g/mol), R is 8.314 J mol⁻¹·K⁻¹, T is the reservoir temperature (433.15 K). Because the deformation of the rock is not taken into account, the rock compressibility C_r is set to 0.

Fig. 16 shows the geometry and boundary conditions of the problem. The values of initial conditions and boundary conditions are set according to the in situ properties of the reservoir under investigation. The initial pore fluid pressure in the gas reservoir is 120 MPa:

$$p(x, y, 0) = 120 \text{ MPa} \tag{5}$$

The negative drainage pressure is specified as 35 MPa, i.e., the

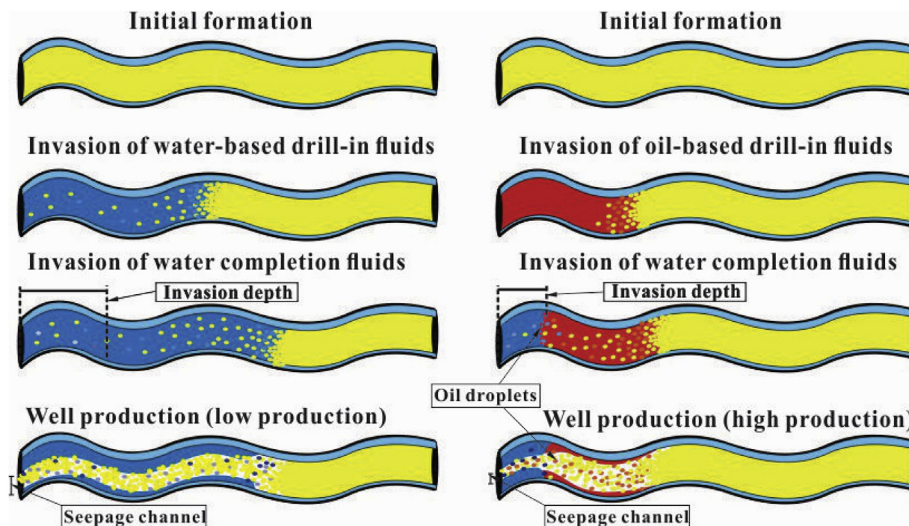


Fig. 15. Schematic diagram of liquid invasion and flowback processes using water or oil-based drill-in fluids and completion fluids.

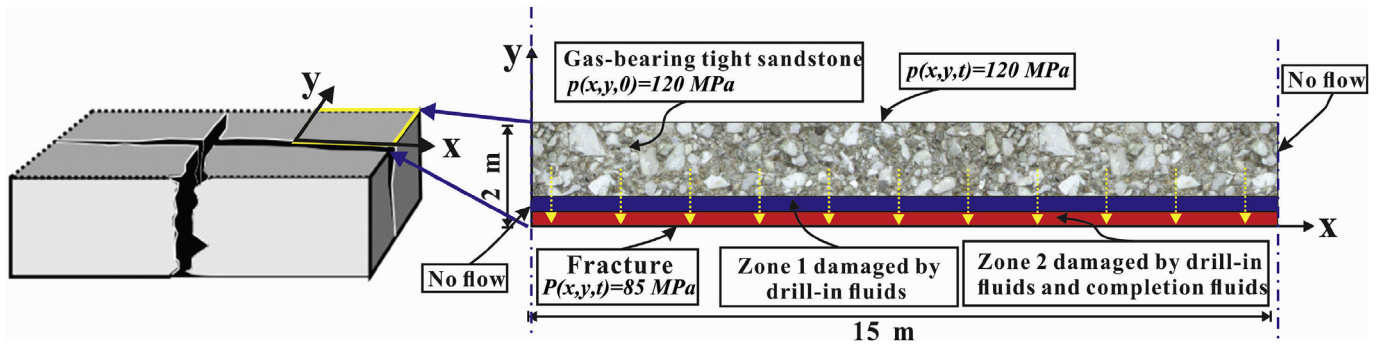


Fig. 16. The geometry, initial conditions and boundary conditions of the computational model.

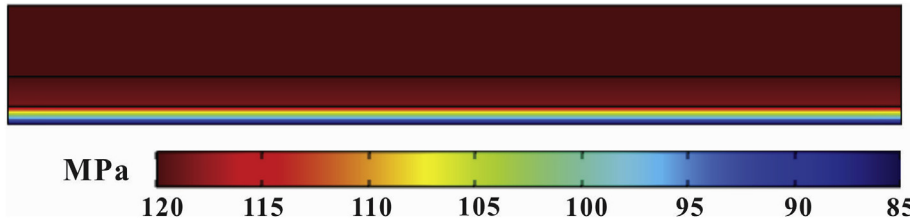


Fig. 17. Zoomed view of computational results from Fig. 16: 2D pore pressure distribution.

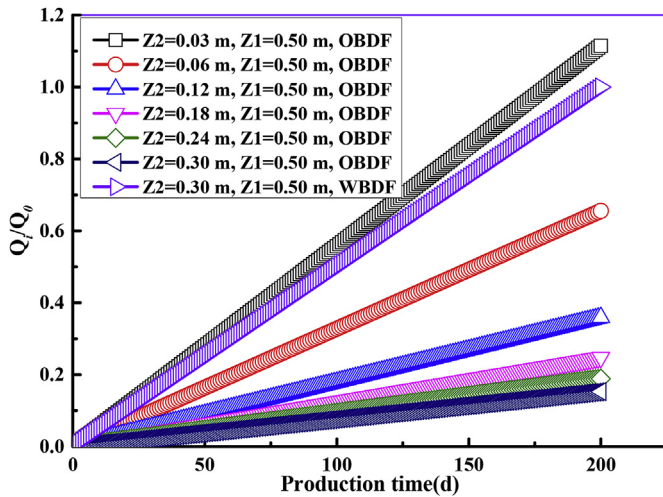


Fig. 18. Comparison of the gas extraction capacity from the matrix to fracture considering different invasion depths of completion fluids.

pressure applied to the fracture surface ($x, y = 0$) is 85 MPa:

$$p(x, y, t)_{y=0} = 85 \text{ MPa} \tag{6}$$

In addition, symmetry boundary conditions were applied on the boundaries with a zero flux condition in y -direction ($x = 0, y$) and ($x = 15m, y$):

$$\frac{\partial p}{\partial n} = 0 \tag{7}$$

The boundary in x -direction ($x, y = 2m$) is the constant pressure boundary, and the pressure is 120 MPa:

$$p(x, y, t)_{y=2} = 120 \text{ MPa} \tag{8}$$

The mechanical and physical parameters used in the study were as follows: porosity (φ) = 0.01; permeability (K_0) = 0.0018 mD. According to the above experimental results, with the invasion of drill-in fluids and completion fluids, the permeability of Zone 1 damaged by OBDF is 0.39 K_0 , the permeability of Zone 2 damaged by OBDF and completion fluids is 0.01 K_0 . The permeability of Zone 1 damaged by WBDF is 0.22 K_0 , while the permeability of Zone 2 damaged by WBDF

and completion fluids is 0.12 K_0 . The width of Zone 1 ($Z1$) is 0.5 m, which is a constant value, and the width of Zone 2 ($Z2$) is a variable. The invasion depth of completion fluids cannot be determined exactly; the experiments in this article cannot determine the permeability of Zone 2 damaged by drill-in fluids and completion fluids. Therefore, the width and permeability of Zone 2 are mostly based on observational experience.

Fig. 17 presents that the change in the pore pressure distribution after 200 days when the width of Zone 2 is 0.3 m. As shown in this figure, the pore pressure tends decrease along the reverse orientation of the y -axis, and the maximum pressure drop occurs in Zone 2.

In addition, the model of the procedure for reducing phase trapping damage by OBDF was simulated for different widths of Zone 2 including 0.03 m, 0.06 m, 0.12 m, 0.18 m, 0.24 m and 0.30 m. The results of the dimensionless cumulative production calculated by the model are shown in Fig. 18. Fig. 18 shows that there is a significant difference between the dimensionless cumulative gas productions with different widths of Zone 2. The cumulative production of the reservoir damaged by OBWF ($Z2 = 0.03 \text{ m}, Z1 = 0.50 \text{ m}$) is significantly larger than that when the reservoir is damaged by WBDF ($Z2 = 0.30 \text{ m}, Z1 = 0.50 \text{ m}$). The simulation results are consistent with the analysis results of the procedure for reducing phase trapping damage by OBDF.

For ultra-deep tight sandstone gas reservoirs in the K9 gas field, the integrated phase trapping damage induced by OBDF should be smaller than the damage induced by WBDF if the invasion depth of the subsequent organic salt completion fluids is shallow enough. The results agree well with the experimental results in this paper and field data obtained by Kang et al. (2018).

5. Conclusions

This paper considers a representative ultra-deep tight sandstone reservoir from the Tarim Basin, NW China as a case study. The geological setting was introduced, and systematic experiments were then carried out to investigate the comprehensive phase trapping damage. The pore microstructure and surface properties were then analyzed. The results revealed how phase trapping damage was caused by drill-in fluids and completion fluids and helped to identify a suitable drill-in fluid system for this reservoir. The following points can be concluded from this work:

- (1) As recorded from the experiments, the *PDR* of the aqueous phase and the hydrocarbon phase in this reservoir were 0.75 and 0.54, respectively. Even when the construction processes, including drilling, drill stem test, completion and well tests were considered, the integrated *PDR* of WBDF (0.99) was more severe than that of OBDF (0.88)
- (2) The results of XRD, SEM, MICP, low-temperature nitrogen adsorption and NMR tests indicated abundant clay minerals, the development of nano-to micron-scale pore throats, multi-scale fractures, abnormally low initial water saturation, oil/water wet, severe fluid invasion and retention. These parameters could all give explanations for the serious phase trapping damage induced by the filtrate of working fluids.
- (3) Analysis showed that OBDF has a larger contact angle and a smaller IFT compared with WBDF, which not only reduces the invasion filtrate volume but also increases the flowback rate. More importantly, the entrapment of an additional third phase induced by OBDF during drilling seems to inhibit the invasion of completion fluids during completion, which minimizes the depth of the damage zone, and thus reduces the comprehensive phase trapping damage.
- (4) A procedure for reducing phase trapping damage by OBDF was presented to describe how the entrapment of the OBDF filtrate affects the integrated phase trapping damage. A numerical simulation model was developed to validate this procedure, and the results indicated that the cumulative production of a reservoir damaged by OBWF-organic salt completion fluids can be larger than that of a reservoir damaged by WBDF-organic salt completion fluids, which further validates the procedure.
- (5) The newly designed experimental technique can assist in the comprehensive evaluation of the phase trapping damage induced by drill-in fluids when the complexity of the operational processes is also included. The results could be useful in understanding and selecting the best drill-in fluids and completion fluids in order to minimize phase trapping damage in ultra-deep tight gas reservoirs.

Acknowledgements

This work was supported by the National Science Foundation of China (No. 51604236; No. 51674209), Sichuan Provincial Research Group of Unconventional Formation Damage Control (No. 2016TD0016) and the China Scholarship Council (CSC No. 201708510127) for a joint Ph.D. fellowship. The authors would like to thank Mrs. Sally Selvadurai for her editing of the manuscript. The authors are grateful for the critical evaluation of the reviewers that lead to significant improvements in the presentation of the results.

Appendix A. Supplementary data

Supplementary data to this article can be found online at <https://doi.org/10.1016/j.petrol.2019.03.045>.

References

- Adamson, A.W., Gast, A.P., 1997. Adsorption of gases and vapors on solids. In: *Physical Chemistry of Surfaces*. John Wiley & Son, New York, pp. 591–681.
- Ahmed Lashari, A., Rehman, K., Hussain, F., Bahrami, H., Shuker, M.T., Kumar, S., 2013. Minimizing phase trapping damage using Malaysian diesel oil. In: Paper SPE 166805 Presented at the SPE/IADC Middle East Drilling Technology Conference & Exhibition. Dubai, UAE, 7–9 October, . <https://doi.org/10.2118/166805-MS>.
- Babadaghi, T., Al-Bemani, A., Boukadi, F., 1999. Analysis of capillary imbibition recovery considering the simultaneous effects of gravity, low IFT, and boundary conditions. In: Paper SPE 57321 Presented at the SPE Asia Pacific Improved Oil Recovery Conference. Kuala Lumpur, Malaysia, 25–26 October, . <https://doi.org/10.2118/57321-MS>.
- Bahrami, H., Rezaee, R., Saeedi, A., Murikhan, G., 2012a. Phase trapping damage in use of water-based and oil-based drilling fluids in tight gas reservoirs. In: Paper SPE 154648 Presented at the SPE Asia Pacific Oil and Gas Conference and Exhibition. Perth, Australia, 22–24 October, . <https://doi.org/10.2118/154648-MS>.
- Bahrami, H., Rezaee, R., Clennell, B., 2012b. Water blocking damage in hydraulically fractured tight sand gas reservoirs: an example from Perth Basin, Western Australia. *J. Pet. Sci. Eng.* 88, 100–106.
- Bennion, D.B., Thomas, F.B., Bietz, R.F., 1996a. Low permeability gas reservoirs: problems, opportunities and solutions for drilling, completion, stimulation and production. In: Paper SPE 35577 Presented at the SPE Gas Technology Symposium. Calgary, Alberta, Canada, 3–5 April, . <https://doi.org/10.2118/35577-MS>.
- Bennion, D.B., Thomas, F.B., Bietz, R.F., Bennion, D.W., 1996b. Water and hydrocarbon phase trapping in porous media-diagnosis, prevention and treatment. *J. Can. Pet. Technol.* 35 (10), 29–36.
- Bennion, D.B., Thomas, F.B., Bietz, R.F., Bennion, D.W., 1999. Remediation of water and hydrocarbon phase trapping problems in low permeability gas reservoirs. *J. Pet. Technol.* 38 (08), 39–48.
- Bennion, D., Thomas, F., Schulmeister, B., Romanova, U., 2006. Water and oil base fluid retention in low permeability porous media - an update. In: Paper PETSOC-2006-136 Presented at the Canadian International Petroleum Conference. Calgary, Alberta, Canada, 13–15 June, . <https://doi.org/10.2118/2006-136>.
- Brunauer, S., Deming, L.S., Deming, W.E., Teller, E., 1940. On a theory of the van der Waals adsorption of gases. *J. Am. Chem. Soc.* 62 (7), 1723–1732.
- Cai, J., Perfect, E., Cheng, C.L., Hu, X., 2014. Generalized modeling of spontaneous imbibition based on Hagen-Poiseuille flow in tortuous capillaries with variably shaped apertures. *Langmuir* 30 (18), 5142–5151.
- Davis, B., Wood, W.D., 2004. Maximizing economic return by minimizing or preventing aqueous phase trapping during completion and stimulation operations. In: Paper SPE-90170 Presented at the SPE Annual Technical Conference and Exhibition. Houston, USA, 26–29 September, . <https://doi.org/10.2118/90170-MS>.
- Fang, J.L., Guo, P., Xiao, X.J., Du, J.F., Dong, C., Xiong, Y.M., Long, F., 2015. Gas-water relative permeability measurement of high temperature and high pressure tight gas reservoirs. *Petrol. Explor. Dev.* 42 (1), 92–96.
- Feng, J., Ren, Q., Xu, K., 2018. Quantitative prediction of fracture distribution using geomechanical method within Kuqa Depression, Tarim Basin, NW China. *J. Pet. Sci. Eng.* 162, 22–34.
- Graham, S.A., Hendrix, M.S., Wang, L.B., Carroll, A.R., 1993. Collisional successor basins of western China: impact of tectonic inheritance on sand composition. *Geol. Soc. Am. Bull.* 105 (3), 323–344.
- Ghanbari, E., Dehghanpour, H., 2015. Impact of rock fabric on water imbibition and salt diffusion in gas shales. *Int. J. Coal Geol.* 138, 55–67.
- Heidaryan, E., Moghadasi, J., Rahimi, M., 2010. New correlations to predict natural gas viscosity and compressibility factor. *J. Pet. Sci. Eng.* 73, 67–72.
- Jerauld, G.R., Salter, S.J., 1990. The effect of pore-structure on hysteresis in relative permeability and capillary pressure: pore-level modeling. *Transport Porous Media* 5 (2), 103–151.
- Kang, Y.L., Zhang, D.J., You, L.J., Wang, Z., Tian, J., 2018. Fluid sensitivity evaluation of ultra-deep tight sandstone gas reservoirs, Tarim Basin. *Oil Gas Geol.* 39 (4), 738–748 (In Chinese).
- Lai, J., Wang, G., Cao, J., Xiao, C., Wang, S., Pang, X., Dai, Q., He, Z., Fang, X., Yang, L., Qin, Z., 2018. Investigation of pore structure and petrophysical property in tight sandstones. *Mar. Petrol. Geol.* 91, 179–189.
- Labani, M.M., Rezaee, R., Saeedi, A., Al Hinai, A., 2013. Evaluation of pore size spectrum of gas shale reservoirs using low pressure nitrogen adsorption, gas expansion and mercury porosimetry: a case study from the Perth and Canning Basins, Western Australia. *J. Pet. Sci. Eng.* 112, 7–16.
- Lee, A.L., Gonzalez, M.H., Eakin, B.E., 1966. The viscosity of natural gases. *J. Pet. Technol.* 18 (8), 997–1000.
- Li, X.C., Kang, Y.L., Haghghi, M., 2018. Investigation of pore size distributions of coals with different structures by nuclear magnetic resonance (NMR) and mercury intrusion porosimetry (MIP). *Measurement* 116, 122–128.
- Lie, K.A., 2014. An Introduction to Reservoir Simulation Using MATLAB: User Guide for the Matlab Reservoir Simulation Toolbox (MRST). SINTEF ICT, Norway, pp. 117–122.
- Liu, Y., Ge, H., Shi, X., Cheng, Y., Zhang, K., Chen, H., Shen, Y., Zhang, J., Qu, X., 2016. The effect of microstructure and rock mineralogy on water imbibition characteristics in tight reservoirs. *J. Nat. Gas Sci. Eng.* 34, 1461–1471.
- Longoria, R.A., Liang, T., Huynh, U.T., Nguyen, Q.P., DiCarlo, D.A., 2017. Water blocks in tight formations: the role of matrix/fracture interaction in hydrocarbon-permeability reduction and its implications in the use of enhanced oil recovery techniques. *SPE J.* 22 (05), 1393–1401.
- Mahadevan, J., Sharma, M., Yortsos, Y.C., 2007. Capillary wicking in gas wells. *SPE J.* 12 (4), 429–437. <https://doi.org/10.2118/103229-PA>.
- Mahmoud, M., 2013. Development of a new correlation of gas compressibility factor (Z-Factor) for high pressure gas reservoirs. *J. Energy Resour. Technol.* 136 (1) 012903-012903.
- Mirzaei-Paiaman, A., Masihi, M., Moghadasi, J., 2011. Formation damage through aqueous phase trapping: a review of the evaluating methods. *Petrol. Sci. Technol.* 29 (11), 1187–1196.
- Roychoudhuri, B., Tsotsis, T.T., Jessen, K., 2013. An experimental investigation of spontaneous imbibition in gas shales. *J. Pet. Sci. Eng.* 111 (11), 87–97.
- Saboorian-Jooybari, H., Pourafshary, P., 2017. Potential severity of phase trapping in petroleum reservoirs: an analytical approach to prediction. *SPE J.* 22 (03), 863–874. <https://doi.org/10.2118/183631-PA>.
- Selvadurai, A.P.S., 2000. *Partial Differential Equations in Mechanics 1: Fundamentals, Laplace's Equation, Diffusion Equation, Wave Equation*. Springer-verlag, Berlin.
- Selvadurai, A.P.S., Najari, M., 2015. Laboratory-scale hydraulic pulse testing: influence of air fraction in cavity on estimation of permeability. *Geotechnique* 65 (2), 126–134.
- Selvadurai, A.P.S., Suvorov, A.P., 2006. *Thermo-poroelasticity and Geomechanics*. Cambridge University Press, Cambridge.
- Selvadurai, A.P.S., Zhang, D.J., Kang, Y.L., 2018. Permeability evolution in natural

- fractures and their potential influence on loss of productivity in ultra-deep gas reservoirs of the Tarim Basin, China. *J. Nat. Gas Sci. Eng.* 58, 162–177.
- Sing, K.S., Williams, R.T., 2004. Physisorption hysteresis loops and the characterization of nanoporous materials. *Adsorpt. Sci. Technol.* 22 (10), 773–782.
- Yang, X., Xu, J., Zhang, Y., Wang, H., Li, W., Wang, L., Wang, L., Fan, W., 2016. Decipher productivity secret to optimise well stimulation for Keshen tight gas reservoir. In: Paper SPE- 181830 Presented at the SPE Asia Pacific Hydraulic Fracturing Conference, Beijing, China, 24-26 August, . <https://doi.org/10.2118/181830-MS>.
- Yao, Y.B., Liu, D.M., 2012. Comparison of low-field NMR and mercury intrusion porosimetry in characterizing pore size distributions of coals. *Fuel* 95, 152–158.
- You, L., Kang, Y., 2009. Integrated evaluation of water phase trapping damage potential in tight gas reservoirs. In: Paper SPE- 122034 Presented at the 8th European Formation Damage Conference, Scheveningen, The Netherlands, 27-29 May, . <https://doi.org/10.2118/122034-MS>.
- You, L., Xue, K., Kang, Y., Liao, Y., Kong, L., 2013. Pore structure and limit pressure of gas slippage effect in tight sandstone. *Sci. World J.* 5, 1–7.
- Zhang, D., Kang, Y., You, L., Li, J., 2019. Investigation of formation damage induced during drill-in process of ultradeep fractured tight sandstone gas reservoirs. *J. Energ. Resour-ASME* 141 (7), 072901.
- Zhou, Z., Abaa, H., Li, X.P., Teklu, T., 2016. Experimental investigation of the effect of imbibition on shale permeability during hydraulic fracturing. *J. Pet. Sci. Eng.* 29, 413–430.
- Zou, C., Zhu, R., Liu, K., Su, L., Bai, B., Zhang, X., Yuan, X., Wang, J., 2012. Tight gas sandstone reservoirs in China: characteristics and recognition criteria. *J. Pet. Sci. Eng.* 88, 82–91.